An Experimental Convective Heat Transfer Investigation Around a Film-Cooled Gas Turbine Blade

C. Camci[1]

T. Arts

von Karman Institute for Fluid Dynamics, RhodeSaint Genèse, Belgium

The present paper deals with an experimental convective heat transfer investigation around a film-cooled, high-pressure gas turbine rotor blade mounted in a stationary, linear cascade arrangement. The measurements were performed in the von Karman Institute Isentropic Light Piston Compression Tube facility. The test blade was made of Macor glass ceramic and was instrumented with thin film gages. The coolant flow was ejected simultaneously through the leading edge (three rows of holes), the suction side (two rows of holes), and the pressure side (one row of holes). The effects of overall mass weight ratio. coolant to free-stream temperature ratio, and free-stream turbulence were successively investigated.

1 Introduction

A classical way to improve the thermal efficiency of a Joule/Brayton cycle is to increase the turbine entry temperature and pressure ratio. As a result, the specific fuel consumption, size, and weight of aero-engines have been significantly reduced during the two last decades. A 25/1 pressure ratio and an 1800 K turbine entry temperature are typical values observed in high-performance jet engines (Olsson, 1982). For such temperatures, efficient blade cooling is most often required to ensure acceptable lifetimes. Over the last few years, a popular method to solve this problem has been discrete hole film cooling.

In the severe engine environment of a film-cooled turbine blade, the large temperature differences existing between the mainstream and the blade surface induce a wall temperature pattern quite different from an adiabatic distribution. Considering, moreover, the important spatial temperature variations due to internal cooling passages and the strongly varying heat flux distribution downstream of a film-cooling hole or slot, the most representative heat transfer parameter seems to be the convective heat transfer coefficient h, defined from the local wall heat flux, the mainstream total or recovery temperature, and the local wall temperature, for given values of the blowing rate m and the coolant temperature. As a matter of fact, either an experimental or a numerical determination of h is essential to perform any detailed heat conduction or thermal stress analysis.

Some of the representative available measurements on film-cooled turbine cascade models were presented by Landon et al. (1972), Nicolas and Le Meur (1974), Ito et al. (1978), Daniels (1979), Dring et al. (1980), Horton et al. (1985), and Camci and Arts (1985a, 1985b). A large number of these heat transfer data, presented either in terms of adiabatic effectiveness or in terms of heat transfer coefficient, are however difficult to use as such for modern cooled gas turbine designs because of the limited range of Reynolds and Mach numbers, as well as gas-to-wall and gas-to-coolant temperature ratios considered in some of these investigations.

The aim of the present experimental heat transfer investigation was to look at the multilocation, discrete hole film cooling of a high-pressure rotor blade mounted in a six-profile, stationary, linear cascade arrangement and subjected to correctly simulated flow conditions, i.e., Mach and Reynolds numbers, as well as free-stream/wall/coolant temperature ratios. The mainstream flow was generated in the von Karman Institute Isentropic Light Piston Compression Tube facility and the coolant flow was ejected simultaneously through the leading edge, the suction side, and the pressure side. The heat transfer distributions were measured over a wide range of coolant to free-stream mass weight and temperature ratios; the influence of free-stream turbulence was also considered.

2 Experimental Apparatus

2.1 Test Facility. A short-duration measurement technique was applied and use was made of the VKI Isentropic Compression Tube facility. The operating principles of this type of wind tunnel were developed about 15 years ago by Jones et al. (1973) and Schultz et al. (1977). A detailed description of the VKI CT-2 facility and of its capabilities was provided by Richards (1980), and Consigny and Richards (1982).

2.2 Model Description. All measurements reported in this paper were carried out along the same rotor blade section as tested by Consigny and Richards (1982). The blade and cascade geometry are described in detail in this reference. The main characteristics are listed as follows:

Chord length: 80 mm
Blade height: 100 mm
Stagger angle: 38.5 deg
Pitch-to-chord ratio: 0.670

[1]Current address: Aerospace Engineering Department, The Pennsylvania State University, University Park, PA 16802.

Contributed by the International Gas Turbine Institute for publication in the JOURNAL OF TURBOMACHINERY. Manuscript received at ASME Headquarters May 1989.

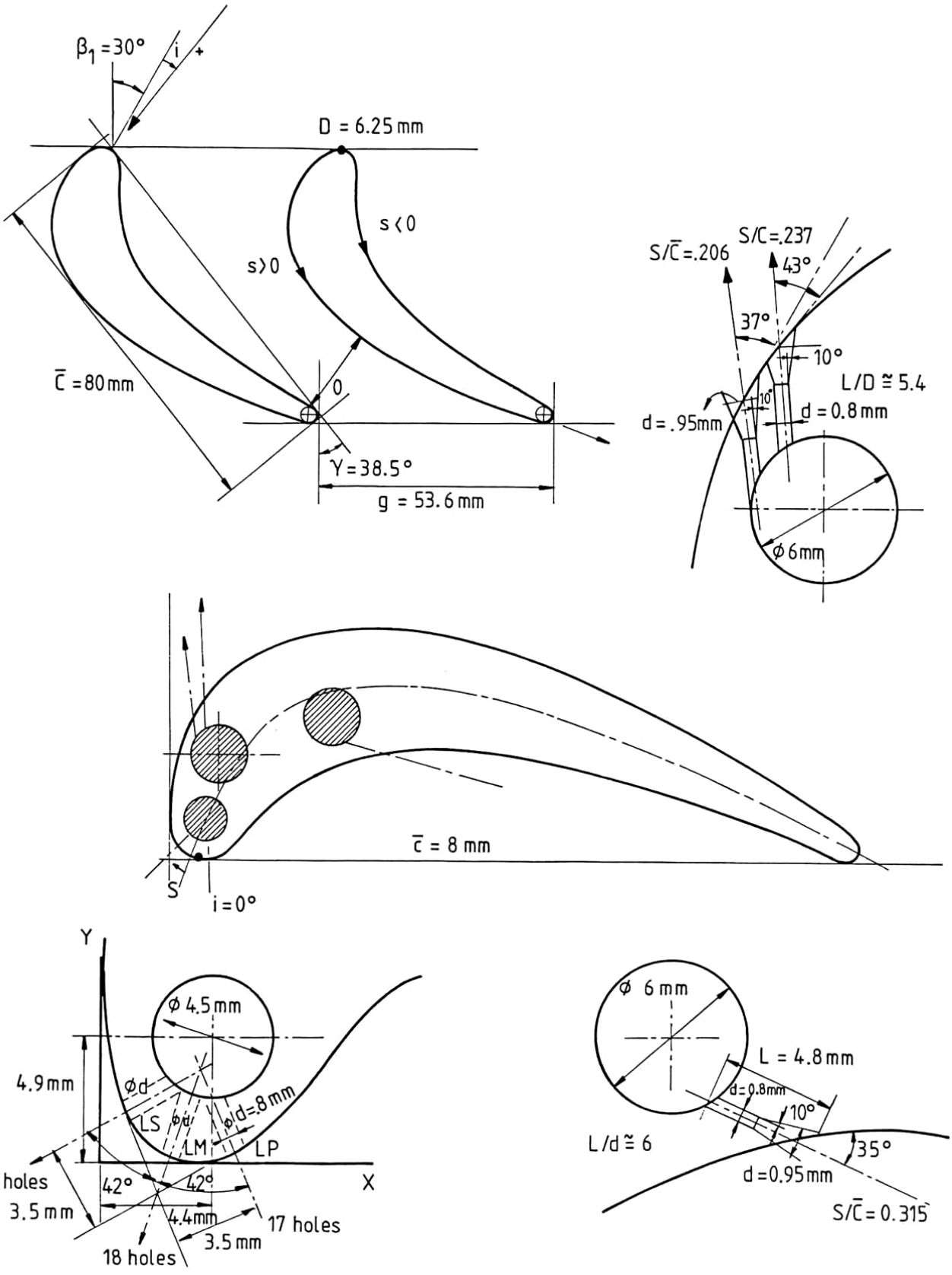
β1 =30°
i
+
D = 6.25 mm
s < 0
s > 0
C̄ =80mm
0
Y=38.5°
g = 53.6 mm
S/C=.237
S/C̄=.206
43°
37°
10°
L/D ≅ 5.4
10°
d=.95mm
d = 0.8 mm
ϕ 6mm
c̄ = 8 mm
S
i=0°
Y
ϕ 4.5mm
4.9mm
ϕd
LS
ϕd
ϕd=.8mm
LM
LP
17 holes
3.5 mm
42°
42°
X
4.4mm
3.5 mm
17 holes
18 holes
ϕ 6 mm
L = 4.8 mm
d=0.8mm
10°
L/d ≅ 6
35°
d=0.95mm
S/C̄= 0.315

FIG. 1

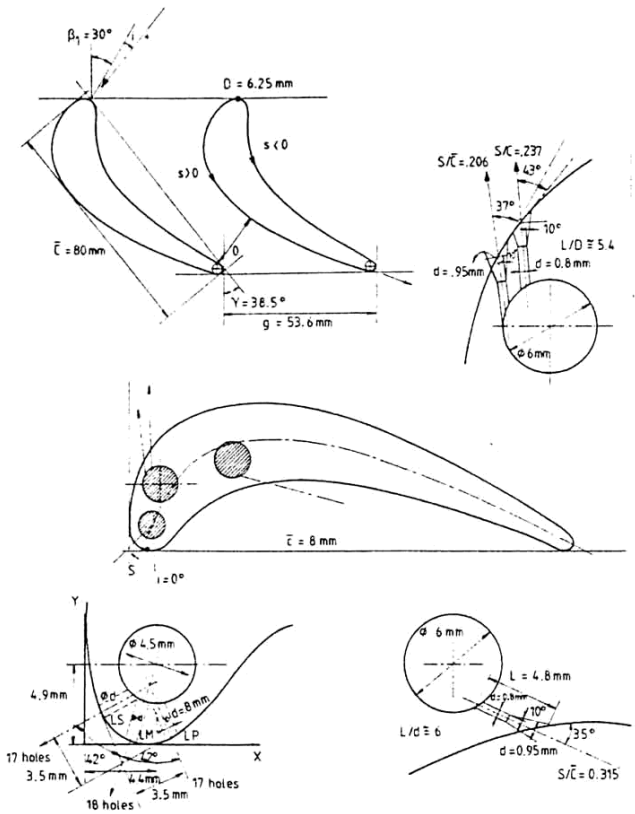

Fig. 1 Cascade geometry and cooling configuration

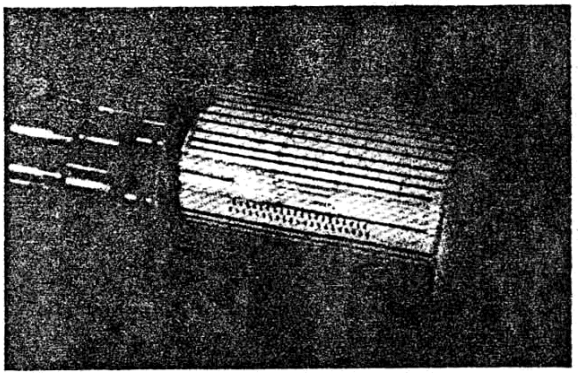

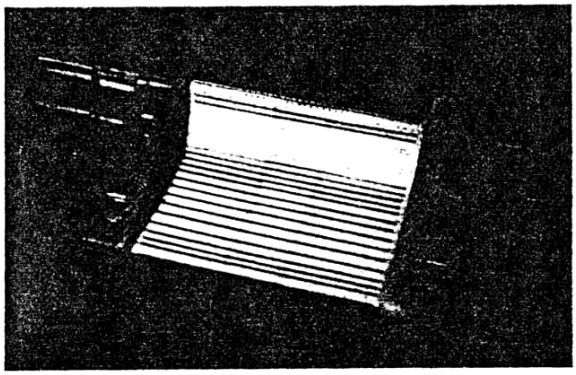

Fig. 2 Heat transfer apparatus

Arcsin (throat/pitch): 21 deg
Design inlet flow angle: 30 deg (referred to axial direction)
Leading edge diameter: 6.25 mm
Trailing edge diameter: 3.0 mm

The cascade consisted of one ceramic and five aluminum airfoils.

The cooling configuration is summarized in Fig. 1. Three rows of cylindrical cooling holes ($d=0.8$ mm; $s/c=-0.031$, 0, 0.031) were located around the leading edge (rows *LP*, *LM*, *LS*). The row and hole spacing were both 2.5 mm. These holes wre spanwise angled at 30 deg from the tangential direction and drilled in a plane perpendicular to the blade surface. Two staggered rows of conical holes ($d=0.8$ mm; $s/c=0.206$, 0.237) were located on the suction side (row *S*). The row and hole spacings were respectively 2.5 and 2.6 mm. These holes were inclined at 37 and 43 deg with respect to the local blade surface and drilled in a plane perpendicular to the blade height. One row of conical holes ($d=0.8$ mm; $s/c=-0.315$) was located along the pressure side (row *P*). The hole spacing was 2.6 mm. These holes were inclined at 35 deg with respect to the local blade surface and drilled in a plane perpendicular to the blade height.

The blade instrumented for heat flux measurements was milled from "Macor" glass ceramic and 45 platinum thin films were applied on its surface (Fig. 2). Three independent cavities were drilled along the blade height to act as plenum chambers. The coolant flow was supplied by a regenerative cryogenic heat exchanger. Pressure tappings and ther-

Nomenclature

c = blade chord
$\overline{C_D}$ = mean value of the discharge coefficient
d = film cooling hole diameter
h = convective heat transfer coefficient
LP, *LM*, *LS* = leading edge film cooling rows of holes (three rows)
M = Mach number
m = blowing rate
$\dot{m}$ = mass flow rate
P = pressure side film cooling row of holes (one row)
p = pressure
Re = Reynolds number
S = suction side film cooling rows of holes (two rows)
s = curvilinear coordinate measured from row *LM* along the blade surface (+ along the suction surface, − along the pressure surface)
T = temperature
T_{ref} = reference temperature (290 K)
Tu = free-stream turbulence intensity = $((\overline{u'^2})^{1/2}/\bar{u})$
u = instantaneous velocity
u' = fluctuating component of velocity
ρ = density

Subscripts

c = related to the cooling flow
is = isentropic
∞ = related to the free-stream flow
0 = related to a stagnation condition
1 = related to the free-stream upstream conditions

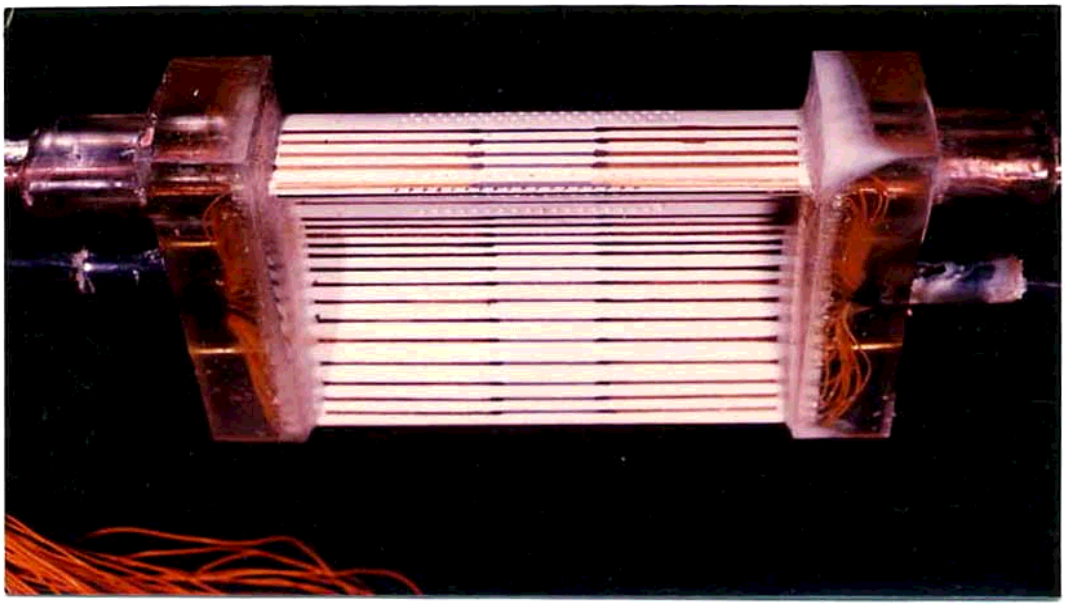

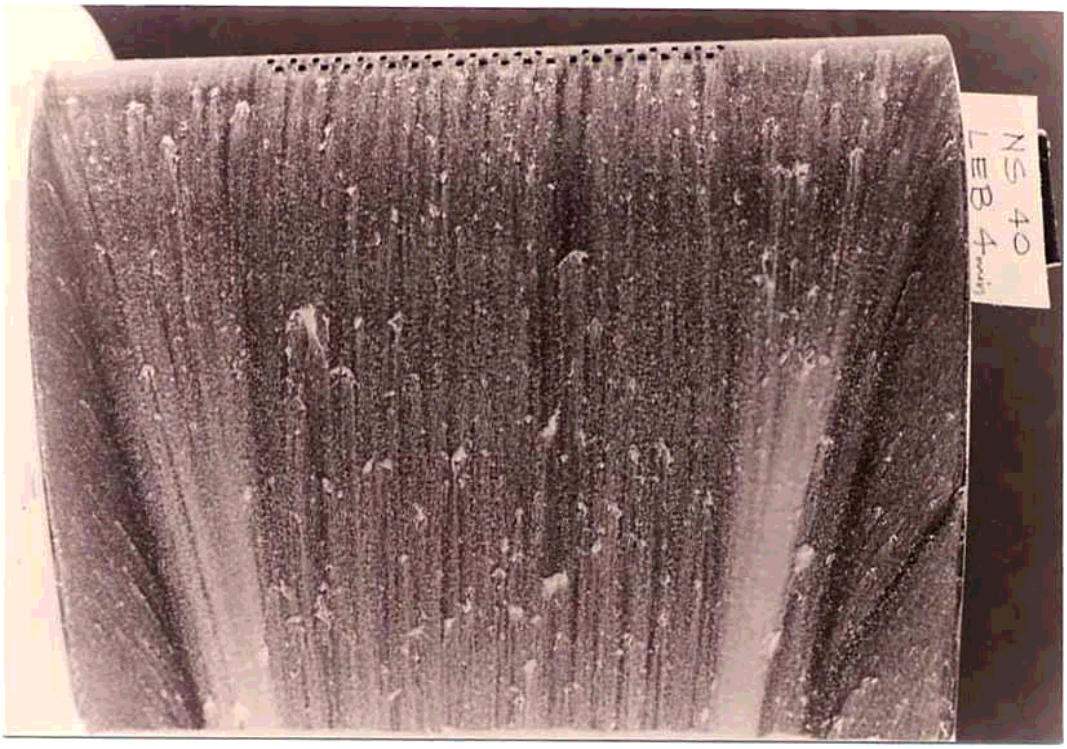
NS 40
LEB 4 min

mocouples continuously provided the coolant characteristics at the entrance and exit of each plenum.

2.3 Measurement Technique. The local wall convective heat flux was deduced from the corresponding time-dependent surface temperature evolution, provided by the platinum thin-film gauges. The wall temperature/wall heat flux conversion was obtained from an electrical analogy, simulating a one-dimensional semi-infinite body configuration. A detailed description of this transient technique was given by Schultz and Jones (1973). The convective heat transfer coefficient is defined as the ratio of the measured wall heat flux and the difference between the free-stream recovery and wall temperatures. A recovery factor equal to 0.896 was used, as if the boundary layer on the blade surface was turbulent everywhere. The uncertainty on the different measured quantities has been estimated as follows, based on a 20:1 confidence interval:

$h = 1000 \text{ W/m}^2\text{K} \pm 50 \text{ W/m}^2\text{K}$
$p = 10^5 \text{ N/m}^2 \pm 750 \text{ N/m}^2$
$T = 100 \text{ K} \pm 1 \text{ K}$
$\dot{m}_c = 0.020 \text{ kg/s} \pm 0.0005 \text{ kg/s}$
$\Sigma \dot{m}_{ci}/\dot{m}_\infty = 2 \pm 0.1$ percent

It should also be realized that the uncertainty associated with the measurements obtained from the two gages located between rows *LS*, *LM*, and *LP* was quite high (~10 . . . 15 percent) as these thin films were affected by undesirable conduction phenomena was well as strong deviations from the assumed one-dimensional heat transfer.

All pressure, temperature, and heat flux measurements were directly acquired by means of a PDP 11/34 computer through one of the VKI data acquisition systems. For the present investigation, the sampling rate was selected to be 1 kHz; the flow duration was about 500 ms. The free-stream total temperature was chosen to be 415 K.

2.4 Free-Stream Turbulence Generation. The free-stream turbulence was generated by a grid of parallel, spanwise-oriented bars. The turbulence intensity was varied by displacing the grid upstream of the cascade; a maximum of 5.2 percent was obtained. The natural turbulence of the facility was about 0.8 percent. The turbulence level, defined in the present paper as $(\overline{u'^2})^{1/2}/\bar{u}$, was measured by means of a VKI constant temperature hot-wire anemometer. The definition of turbulence spectrum could not be carried out for practical reasons. These measurements are currently underway and will be reported in a later paper.

3 Free-Stream Flow Characteristics

The isentropic Mach number distribution measured along the blade profile at zero incidence and without film cooling is shown in Fig. 3. The isentropic outlet Mach number selected for this investigation was chosen equal to 0.925. The flow accelerated quite regularly along the suction side up to transonic conditions close to the trailing edge. Along the pressure side, a velocity peak was predicted at $s/c = -0.08$. Farther downstream, the favorable pressure gradient accelerated the flow up to the trailing edge. Because of the small leading edge radius, detailed static pressure measurements could unfortunately not be carried out around the stagnation point position.

A two-dimensional inviscid time-marching program (Arts, 1982) provided a valuable prediction of this velocity distribution (Fig. 3). Because of the weakness of this type of approach in accurately determining the stagnation point position, a singularity method (Van den Braembussche, 1973) was also used around the leading edge. Both calculation methods were inviscid and no attempt was made to simulate the effect of film cooling. At zero incidence, the stagnation point position

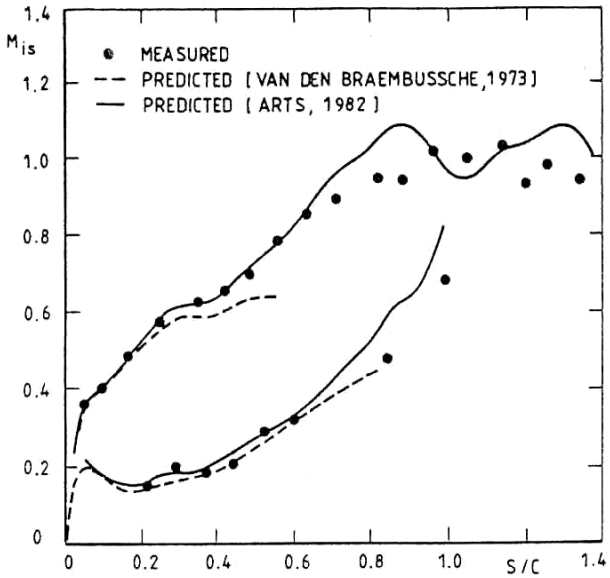

Fig. 3 Blade velocity distribution

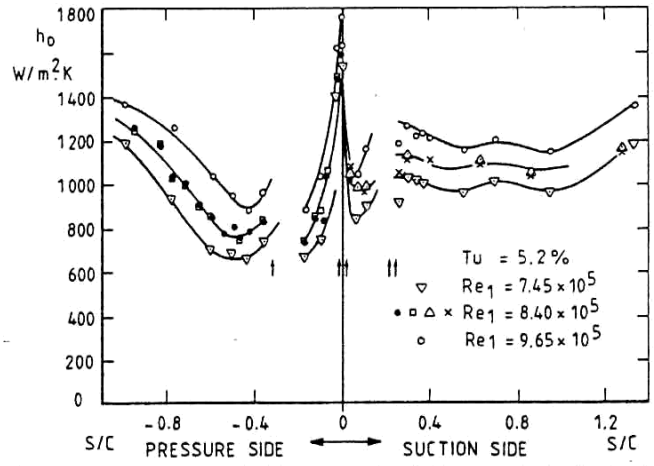

Fig. 4 Heat transfer distribution without film cooling: effect of Reynolds number

was calculated to be at $s/c = -0.019$ (on the pressure side), between rows *LM* and *LP*. This result suggested that the suction side boundary layer would be affected by rows *LM* and *LS* whereas the pressure side boundary layer would only be affected by row *LP*. This behavior was confirmed from the detailed heat transfer measurements conducted by Camci and Arts (1985a) around the leading edge.

4 Heat Transfer Without Film Cooling

The convective heat transfer coefficient distributions measured at zero incidence, and without any coolant emission, are shown in Fig. 4 for three free-stream Reynolds number (based on chord length and upstream conditions) values. Possible undesirable free-stream air recirculation was avoided by filling the three plenum chambers with flexible inserts. In the absence of the inserts, as was demonstrated from oil flow visualizations (Camci, 1985), free-stream air entered into the leading edge plenum through row *LM* and was ejected through rows *LS* and *LP*, influencing the local heat transfer rates. The same phenomenon was observed across the two suction side rows (*S*).

The highest wall heating rates were measured in the leading edge region; a detailed investigation of this area, without and with film cooling, was presented by Camci and Arts (1985a).

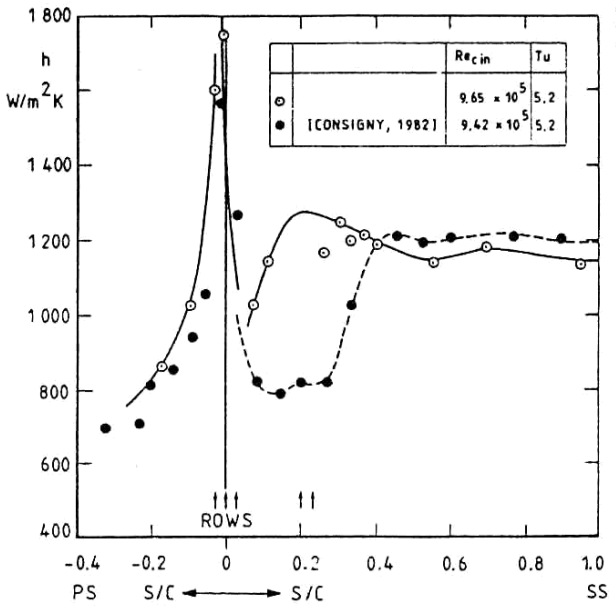

Fig. 5 Heat transfer distribution without film cooling: effect of cooling holes

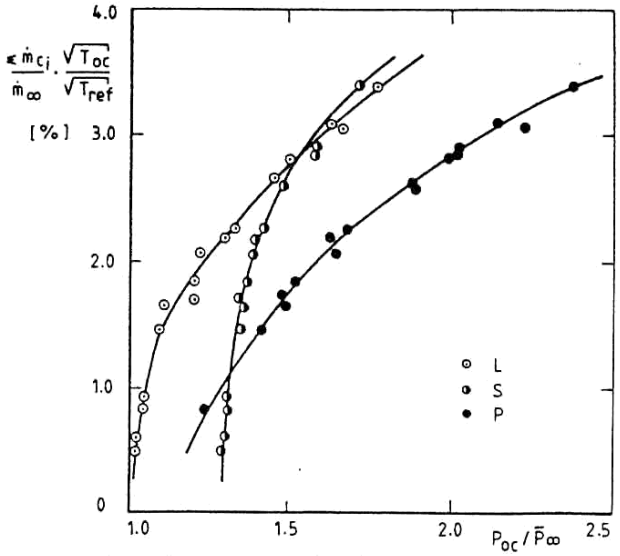

Fig. 6 Normalized total coolant mass flow rate

Figure 5 demonstrates a definite influence of the existence of rows *LM* and *LS* on the suction side boundary layer behavior between $s/c = 0.0$ and 0.22. The results from the present model (open symbols) were obtained without any coolant flow emission, the plenum cavities being filled with the inserts previously mentioned; the free-stream turbulence intensity was equal to 5.2 percent. The comparison between the present data and those obtained by Consigny and Richards (1982) (closed symbols) for the same turbulence intensity around an identical but smooth, undrilled blade, reveals indeed an earlier transition. Along the pressure side, an eventual tripping effect of row *LP* is not as obvious; similar heat transfer distributions were measured along the present blade and that of Consigny and Richards. As a matter of fact, the early pressure side boundary layer transition is principally due to the existence of the velocity peak and the curvature inversion.

The boundary layers developing along the suction and pressure surfaces are much thinner than the diameter of the emission holes. The boundary layer thickness, computed at the location of row *S* by means of a two-dimensional boundary layer program (Crawford et al., 1980) is about five times smaller than the hole diameter; this corresponds to a local value of the hole diameter to momentum thickness ratio equal to 43, representative of a real configuration. One direct consequence of this situation is that such a boundary layer most probably undergoes a local separation and reattachment over the rows of emission. This behavior is exemplified by the data scatter observed in Fig. 4 over rows *S* and *P*.

5 Coolant Flow Characteristics

5.1 Total Coolant Mass Flow Rate. The coolant flow across rows *S*, *L*(*S*, *M*, *P*), and *P* originated from a single reservoir through a heat exchanger providing the required coolant to free-stream temperature ratios. This implied that the total coolant mass flow rate $\Sigma\dot{m}_{ci}$, measured across a single choked orifice, was shared among the suction side, leading edge, and pressure side plenum chambers. The amount of coolant passing through each of these cavities had therefore to be calculated in order to evaluate local values of coolant to free-stream mass weight ratio and blowing rate. The first step was to establish a unique dependency between $\Sigma\dot{m}_{ci}$ and the local coolant to free-stream static pressure ratio (Fig. 6). A normalized overall mass weight ratio $(\Sigma\dot{m}_{ci}/\dot{m}_\infty)\ (T_{oc}/T_{ref})^{1/2}$ was therefore defined from $\Sigma\dot{m}_{ci}$, pressure and temperature measurements in each plenum, and free-stream static pressure at each row of emission; $\dot{m}_\infty$ is the free-stream mass flow through one blade passage. All the measurements were taken for three different values of the coolant to free-stream temperature ratio ($T_{oc}/T_{o_\infty} = 0.7, 0.6, 0.5$).

5.2 Discharge Coefficient. The second step was to determine local values of the discharge coefficient. Averaged values of this parameter were obtained (Fig. 7) at the location of rows *S*, *L* (*S*, *M*, *P*), and *P* from independent film cooling investigations performed by Camci and Arts (1985a, 1985b). Significant losses were observed across the leading edge holes compared to the two other emission sites. These values showed, nevertheless, qualitative agreement with data presented by Tillman et al. (1984), obtained in an incompressible flow (water tunnel) situation. The relatively low C_D values measured in the leading edge region were expected to occur because of the highly complicated nature of the coolant flow, with compound angle emission. Across the pressure and suction side rows, C_D values varied between 0.4 and 0.5.

5.3 Coolant Flow Distribution Among the Emission Rows. The third and final step was the quantitative determination of the coolant mass flow rate through each ejection site. It was obtained by combining data from Figs. 6 and 7. The coolant to free-stream static pressure ratio for each plenum was obtained from Fig. 6, knowing the measured total mass flow rate $\Sigma\dot{m}_{ci}$. The isentropic mass flow rate across the corresponding film cooling rows was then calculated. The application of the corresponding discharge coefficient values (Fig. 7) finally provided the three real mass flow rates, characterized by the parameter $\dot{m}_{ci}/\Sigma\dot{m}_{ci}$ (Fig. 8). For very low pressure ratios, the flow conditions were not well defined in the leading edge plenum and very low C_D values were responsible for quite low local mass flow rates. The cooling rows *S* and *P* then performed the largest percentage of the emission. However, for a typical value of the overall mass weight ratio ($\Sigma\dot{m}_{ci}/\dot{m}_\infty = 3$ percent), the coolant split was found to be 40 percent/35 percent/25 percent, respectively, through the leading edge, suction, and pressure side emission rows.

5.4 Local Blowing Rate Evolution. The local blowing rate variations (Fig. 9) were determined from the three emission mass flow rate distributions (Fig. 8), the corresponding emission surfaces (Fig. 1), and the local free-stream conditions

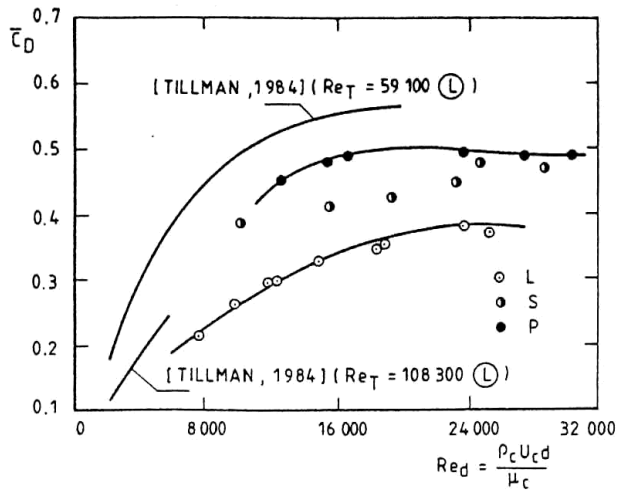

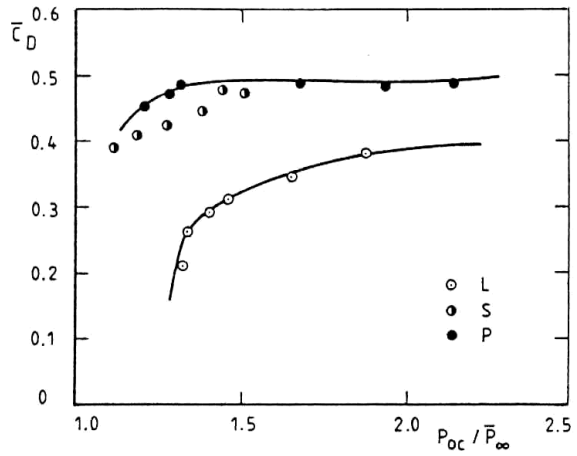

Fig. 7 Discharge coefficient distribution

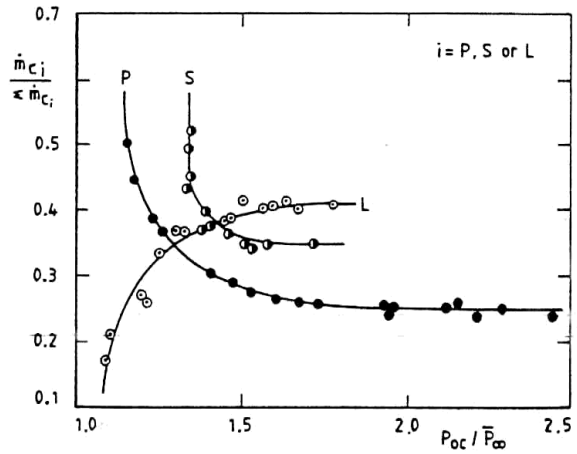

Fig. 8 Coolant flow distribution

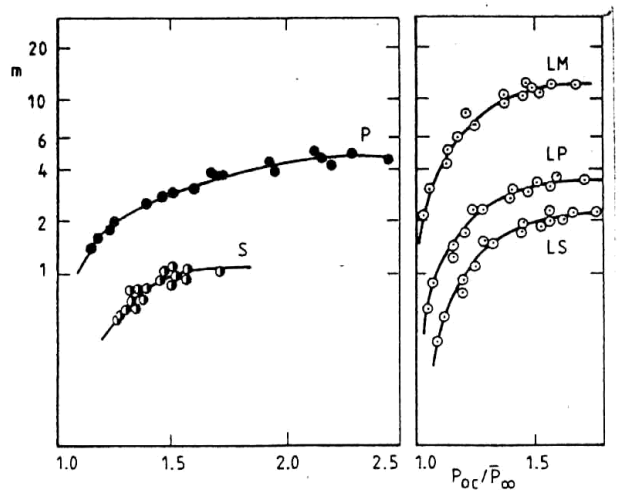

Fig. 9 Local blowing rate evolution

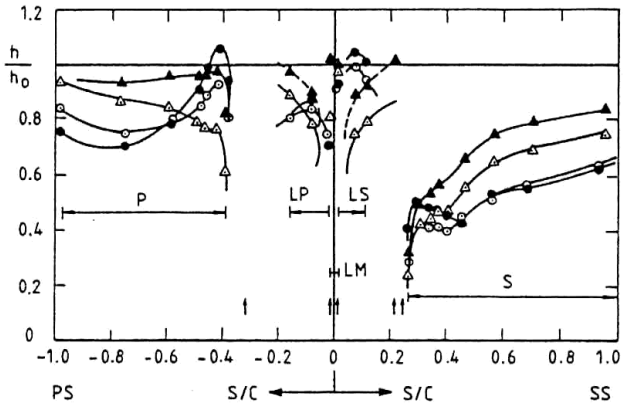

	$\Sigma \dot{m}_{ci}/\dot{m}_\infty$	$T_{oc}/T_{o\infty}$	m_p	m_{LP} / P^*	m_{LM} / P^*	m_{LS} / P^*	m_s
▲	0.50%	0.71	1.42	1.004	0.984	1.038	0.59
△	0.93%	0.71	1.94	1.022	1.002	1.056	0.62
⊙	2.07%	0.70	3.03	1.74 / 1.21	5.98 / 1.19	1.11 / 1.25	0.72
●	3.09%	0.70	4.17	3.20 / 1.58	11.0 / 1.55	2.05 / 1.63	0.93

$P^* = P_{oc}/\bar{P}_\infty$

Fig. 10 Heat transfer distribution with film cooling: effect of overall mass weight ratio

(Fig. 3). The data of Fig. 9 are representative for three different coolant to free-stream total temperature ratios ($T_{oc}/T_{c_\infty} = 0.7$, 0.6, and 0.5). The scatter is mainly due to the measurement difficulties associated with the lowest temperature ratio ($T_{oc}/T_{o_\infty} = 0.5$; $T_{oc} \cong 200$ K).

6 Heat Transfer With Film Cooling

The heat transfer measurement with film cooling were performed for constant values of the downstream Reynolds (2.32×10^6; based on chord length and downstream isentropic conditions) and isentropic Mach (0.925) numbers. The overall mass weight ratio ($\Sigma \dot{m}_{ci}/\dot{m}_\infty$) was varied between 0.5 and 3.3 percent and coolant to free-stream temperature ratios (T_{oc}/T_{o_∞}) ranging between 0.51 and 0.70 were considered.

6.1 Effect of Overall Mass Weight Ratio. The results presented in this section were obtained for a coolant to free-stream temperature ratio equal to 0.70. The effect of overall mass weight ratio variations is demonstrated in Fig. 10. Downstream of row *LS*, the heat transfer coefficient distribution was observed to be quite smooth for low values of $\Sigma \dot{m}_{ci}/\dot{m}_\infty$ (0.50, . . . , 0.93 percent). As expected, increasing values of the mass weight ratio resulted in lower wall convective heat fluxes. For higher values (2.07, . . . , 3.09 percent) however, a continuously increasing heat transfer coefficient was measured around $s/c = 0.08$. This behavior was explained by the higher blowing rate values (up to 2.05) observed along this highly curved surface; the effect of the coolant film was

more to augment the local free-stream turbulence, and hence heat transfer in this not yet fully turbulent region, than to protect the surface efficiently.

Downstream of row *LP*, similar behavior was observed for the different values of the overall mass weight ratio. An additional effect might be due to the existence of the pressure side curvature inversion; the latter induced the reattachment ($s/c = -0.16$) of the coolant layers, separated from the wall at the high blowing rate values.

Downstream of row *S*, different phenomena were identified. For low values of $\Sigma\dot{m}_{ci}/\dot{m}_\infty$ (0.5, . . . , 0.93 percent), significant difference was observed in heat flux levels, although the row *S* blowing rate variation was rather limited (0.59, . . . , 0.62). This behavior was explained by a cumulative effect, due to the additional contribution of the leading edge films (rows *LM*+*LS*), more effective for the highest value of the overall mass weight ratio (0.93 percent). For even higher values (2.07, . . . , 3.09 percent), a more and more significant heat transfer coefficient increase was measured downstream of row *S*. This phenomenon, due to the strong jet/mainstream interaction, was spread over a length equal to almost 30 film-cooling hole diameters. No significant differences were observed farther downstream.

Downstream of row *P*, two regions had to be considered. Just downstream of the cooling holes, the heat transfer coefficient first decreased with increasing overall mass weight ratio (0.5, . . . , 0.93 percent). For higher values (2.07, . . . , 3.09 percent) the classical heat transfer augmentation took place. Farther downstream, on the contrary, the lowest heat transfer coefficient values were observed for the highest values of $\Sigma\dot{m}_{ci}/\dot{m}_\infty$. This was most probably due to the concave nature of the wall; the free-stream pulled the separated jets back to the wall.

6.2 Effect of Coolant to Free-Stream Temperature Ratio. Values of the coolant to free-stream temperature ratio as low as 0.5 are most usually observed in advanced aero-engines. In order to identify the effect of this important parameter, measurements were taken for three different values (0.7, 0.56, and 0.51), while $\Sigma\dot{m}_{ci}/\dot{m}_\infty$ was maintained at a constant value of about 3.1 percent. The results presented in Fig. 11 were obtained.

As obviously expected, significant heat transfer coefficient reductions were obtained when lowering the coolant temperature. The only exception was observed along the suction side front part, just downstream of row *LS*. This phenomenon was explained by the very high local blowing rate value, causing a separation of the coolant film. Just downstream of rows *P*, *LP*, and *S*, although local blowing rates were maintained at constant values, the importance of the wall heat flux augmentation identified in the preceding paragraph decreased with T_{oc}. As a matter of fact, a decrease of the temperature ratio (T_{oc}/T_{o_∞}) results in an increase of the density ratio (ρ_c/ρ_∞) and hence, for a constant blowing rate, a decrease of the velocity ratio (u_c/u_∞) and moreover of the momentum ratio ($\rho_c u_c^2/\rho_\infty u_\infty^2$). The penetration of a "colder" film in the boundary layer was thus less severe; in other words, the turbulence augmentation just downstream of these film cooling rows was less important.

6.3 Effect of Free-Stream Turbulence Intensity. The effect of free-stream turbulence was also investigated in the presence of film cooling (Fig. 12). The turbulence level was varied from 0.8 to 5.2 percent while maintaining almost constant values of $\Sigma\dot{m}_{ci}/\dot{m}_\infty$ (~2.5 percent) and T_{oc}/T_{o_∞} (~0.5). The values of h and h_o plotted in Fig. 12 were obtained for equal values of the turbulence intensity. No significant changes in the wall heat flux were observed when varying Tu. As a matter of fact, this behavior was expected because of the dominant effect of the coolant flow (almost a new boundary layer) just downstream of the emission rows and of the turbulent nature of the boundary layers developing along the suction and pressure surfaces.

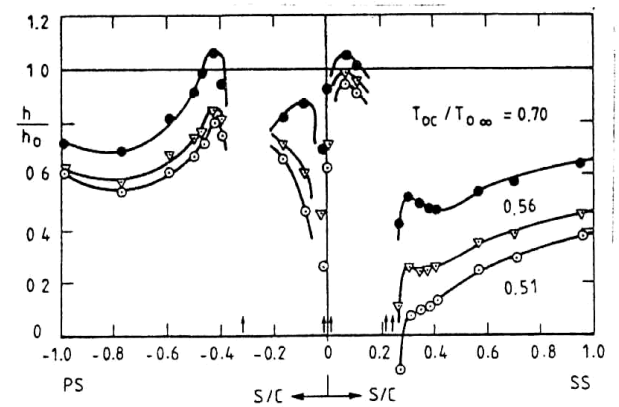

	$\frac{\Sigma\dot{m}_{ci}}{\dot{m}_\infty}$	T_{oc}/T_{o_∞}	mp	m_{LP} / p^*	m_{LM} / p^*	m_{LM} / p^*	m_S
●	3.09%	0.70	4.17	3.20 / 1.58	11.0 / 1.55	2.05 / 1.63	0.93
▽	3.32%	0.56	4.67	3.36 / 1.53	11.5 / 4.50	2.15 / 1.58	0.99
⊙	3.12%	0.51	4.37	3.02 / 1.41	10.4 / 1.38	1.93 / 1.46	0.98

$P^* = P_{oc}/\bar{P}_\infty$

Fig. 11 Heat transfer distribution with film cooling: effect of temperature ratio

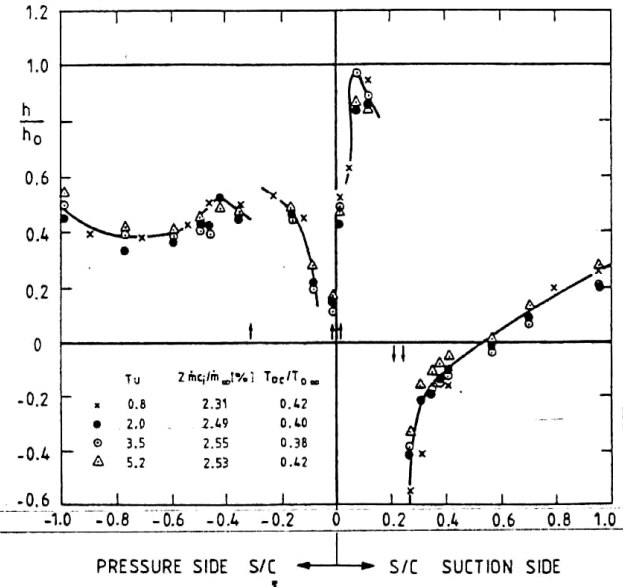

Fig. 12 Heat transfer distribution with film cooling: effect of turbulence intensity

7 Conclusions

Detailed convective heat transfer measurements were obtained for a high-pressure, film-cooled rotor blade mounted in a stationary cascade arrangement and submitted to correctly simulated aero-engine conditions (Mach and Reynolds numbers as well as temperature ratios). The effects of overall mass weight ratio, coolant to free-stream temperature ratio, and free-stream turbulence intensity were successively investigated.

The main conclusions of this investigation are:

- In the absence of coolant emission, the suction side boundary layer was dominated by the existence of the leading edge film cooling holes, while the pressure side boundary layer behavior was dominated by the free-stream pressure gradient. Moreover, the influence of free-stream turbulence on the heat transfer coefficient distribution was extremely limited;
- film cooling around the leading edge proved to be quite effective for low overall mass weight ratio values. The same conclustion was drawn downstream of rows S and P. For higher values of $\Sigma \dot{m}_{ci}/\dot{m}_{\infty}$, increases in local heat transfer were measured just downstream of the various film cooling rows;
- the convective heat transfer coefficient distribution proved to be strongly dependent on the coolant to free-stream temperature ratio; no significant effect of free-stream turbulence was identified.

References

Arts, T., 1982, "Cascade Flow Calculation Using a Finite Volume Method," in: *Numerical Methods for Flow in Turbomachinery*, von Karman Institute Lecture Series, 1982-05.

Camci, C., and Arts, T., 1985, "Experimental Heat Transfer Investigation Around the Film-Cooled Leading Edge of a High-Pressure Gas Turbine Rotor Blade," ASME *Journal of Engineering for Gas Turbines and Power*, Vol. 107, No. 4, pp. 1016–1021.

Camci, C., and Arts, T., 1985, "Short Duration Measurements and Numerical Simulation of Heat Transfer Along the Suction Side of a Film-Cooled Turbine Blade," ASME *Journal of Engineering for Gas Turbines and Power*, Vol. 107, No. 4, pp. 991–997.

Camci, C., 1985, "An Experimental and Theoretical Heat Transfer Investigation of Film Cooling on a High Pressure Gas Turbine Blade," Ph.D. Thesis, Katholieke Universiteit Leuven, Belgium.

Consigny, H., and Richards, B. E., 1982, "Short Duration Measurements of Heat Transfer Rate to a Gas Turbine Blade," ASME *Journal of Engineering for Power*, Vol. 104, No. 3, pp. 542–551.

Crawford, M. E., Kays, W. M., and Moffat, R. J., 1980, "Full Coverage Film Cooling. Part II: Heat Transfer Data and Numerical Simulation," ASME *Journal of Engineering for Power*, Vol. 102, No. 4, pp. 1006–1012.

Daniels, L. C., 1979, "Film Cooling of Gas Turbine Blades," Ph.D. Thesis, University of Oxford, United Kingdom.

Dring, R. P., Blair, M. F., and Joslyn, H. D., 1980, "An Experimental Investigation of Film Cooling on a Turbine Rotor Blade," ASME *Journal of Engineering for Power*, Vol. 102, No. 1, pp. 81–87.

Horton, F. G., Schultz, D. L., and Forest, A. E., 1985, "Heat Transfer Measurements With Film Cooling on a Turbine Blade Profile in Cascade," ASME Paper No. 85-GT-117.

Ito, S., Goldstein, R. J., and Eckert, E. R. G., 1978, "Film Cooling of a Gas Turbine Blade," ASME *Journal of Engineering for Power*, Vol. 100, pp. 476–481.

Jones, T. V., Schultz, D. L., and Hendley, A. D., 1973, "On the Flow in an Isentropic Free Piston Tunnel," ARC R&M 3731.

Lander, R. D., Fish, R. W., and Suo, M., 1972, "External Heat Transfer Distribution of Film Cooled Turbine Vanes," *Journal of Aircraft*, Vol. 9, No. 10, pp. 707–714.

Nicolas, J., and Le Meur, A., 1974, "Curvature Effects on a Turbine Blade Cooling Film," ASME Paper No. 74-GT-156.

Olsson, U., 1982, "Advanced Engine Technology and Its Influence on Aircraft Performance," *Journal of Aircraft*, Vol. 19, No. 5, pp. 380–384.

Richards, B. E., 1980, "Heat Transfer Measurements Related to Hot Turbine Components in the von Karman Institute Hot Cascade Tunnel," in: *Testing and Measurement Techniques in Heat Transfer and Combustion*, AGARD CP 281, Paper 6.

Schultz, D. L., and Jones, T. V., 1973, "Heat Transfer Measurements in Short Duration Hypersonic Facilities," AGARDograph 165.

Schultz, D. L., Jones, T. V., Oldfield, M. L. G., and Daniels, L. C., 1977, "A New Transient Facility for the Measurement of Heat Transfer Rates," in: *High Temperature Problems in Gas Turbine Engines*," AGARD CP 229, Paper 31.

Tillman, E. S., Hartel, E. L., and Jen, H. F., 1984, "The Prediction of Flow Through Leading Edge Holes in a Film Cooled Airfoil With and Without Inserts," ASME Paper No. 84-GT-4.

Van Den Braembussche, R., 1973, "Calculation of Compressible Subsonic Flow in Cascades With Varying Blade Height," ASME *Journal of Engineering for Power*, Vol. 95, No. 4, pp. 345–351.